Inorganica Chimica Acta 490 (2019) 163–172

Contents lists available at ScienceDirect

Inorganica Chimica Acta

journal homepage: www.elsevier.com/locate/ica

Research paper

Biomimetic catalytic activity and structural diversity of cobalt complexes with N_3O-donor Schiff base ligand

Narayan Ch. Jana[a,1], Moumita Patra[a,1], Paula Brandão[b], Anangamohan Panja[a,*]

[a] Postgraduate Department of Chemistry, Panskura Banamali College, Panskura RS, WB 721152, India
[b] Department of Chemistry, CICECO-Aveiro Institute of Materials, University of Aveiro, 3810-193 Aveiro, Portugal

ARTICLE INFO

Keywords:
Biomimetic catalysis
Intermediate
Cobalt complexes
Crystal structures
Mass spectrometry and mechanism

ABSTRACT

This report describes the syntheses and structural characterizations of four new cobalt(III) compounds (**1–4**) derived from a tetradentate Schiff base ligand and their catalytic oxidation of different *o*-aminophenols in aerobic condition. X-ray crystal structural studies reveal that both pseudohalide ions and solvents used for the syntheses have significant influence on the structural diversity in these systems. All these compounds show the diverse catalytic activity towards the aerial oxidation of different o-aminophenols. As expected, the substitutionally labile coordination sites available for substrate binding is responsible for significantly higher catalytic activity of **1** and **2** then others. Literature reports reveal that although significant attention has been made to the catalytic oxidation of some substituted *o*-aminophenols in terms of the isolations and characterizations of their oxidised products with the native enzyme and its models, but the detailed kinetic studies were not available in the literature. Herein, we have examined the detailed kinetic studies of the aerobic oxidation of two substituted *o*-aminophenols, namely 2-amino-5-methylphenol and 2-amino-4-methylphenol, using **1** and **2** as catalysts. ESI mass spectrometry provides significant information to get insight into the mechanistic details and further disclose that the methyl substation in aromatic ring does not inhibit formation of the complex-substrate aggregate but it resulted the phenoxazine chromophore instead of phenoxazinone chormophore.

1. Introduction

Metal complexes of Schiff base ligands have gained considerable attention because of their synthetic simplicity, ease of tunability of their stereo-electronic structures, and notable biological activities [1–3], catalytic activities [4–9], fluorescence properties [10–12], applications in sensors [13], etc. Remarkably, the Schiff base ligands readily form stable complexes with most of the transition metals [14,15], Schiff base complexes of first row transition metals provided us numerous efficient structural and functional models of various metalloproteins and metalloenzymes. We have been working for last few yours in modeling the structures and functions of two important metallo-oxidases, namely phenoxazinone synthase and catechol oxidase. Phenoxazinone synthase [16–18] functions in the final step of biosynthesis of natural antibiotic actinomycin D, where two molecules of substituted *o*-aminophenols are oxidatively coupled to form phenoxazinone chromophore through catalytic activation of dioxygen [19]. That naturally occurring antibiotic is used clinically for the treatment of many tumors including Wilm's tumor, where the phenoxazinone chromophore inhibits the RNA synthesis by intercalating the DNA base pairs [20,21]. Model studies of such metalloenzymes are worthy as that may help in unravelling the catalytic mechanism of action of these enzymes by means of a synthetic analogue approach. Moreover, the efficient functional models could be the alternative of traditional oxidants, such as permanganates, dichromate and heavy metal oxides, used industrially in the production of various desired organic and pharmaceutical compounds, resulting in huge wastes and causing environmental pollution. Model studies of phenoxazinone synthase [22–24] were mainly carried out with simple *o*-aminophenol [25–33], while other aminophenol derivatives have not been examined well. Recently, Tomoda and co-workers reported the antibacterial effects of Phx-1 (2-aminophenoxazin-3-one), Phx-2 (2-amino-4,4a-dihydro-4a-7- dimethyl-3*H*-phenoxazin-3-one), and Phx-3 (3-amino-1,4a-dihydro-4a-8-dimethyl-2*H*phenoxazin- 2-one) (Scheme 1), which were produced by the reaction of *o*-aminophenol or its derivatives with bovine hemoglobin [34]. Thus, the chemistry of phenoxazine derivatives is worthy to be further explored.

Nature has mainly opted copper and iron for the active sites of the metallo-oxidases for their biological functions [35,36]. Although,

* Corresponding author.
E-mail address: ampanja@yahoo.co.in (A. Panja).
[1] These authors contributed equally to this work.

https://doi.org/10.1016/j.ica.2019.03.017
Received 4 February 2019; Received in revised form 9 March 2019; Accepted 12 March 2019
Available online 13 March 2019

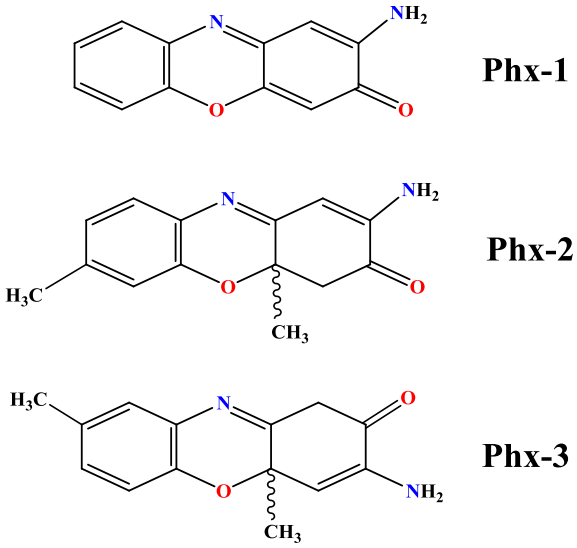

Scheme 1. Chemical structures of Phx-1, Phx-2, and Phx-3.

cobalt has comparable redox flexibility like copper and iron, but it has not been chosen for the active site in any metallo-oxidase. The substitutionally inert character of cobalt especially in cobalt(III) state is main reason behind its exclusion form such metalloenzymes. However, this inert character could be helpful in detecting the intermediates species formed in the catalytic cycle through various instrumental techniques, which in turn may help to better understanding the mechanistic pathway of a catalytic reaction [37–39]. With this aim, we intended to develop some cobalt complexes with Schiff base ligands for *in vitro* catalytic studies, modeling the functions of metallo-oxidases that may give us significant information in unraveling the catalytic mechanism. We have started systematic development of coordination chemistry with Schiff bases derived from a triamine *N,N*-dimethyldipropylenetriamine, protected at one end for Schiff base condensation; the coordination chemistry of which is almost unexplored [40,41]. In the present endeavor, we employed Schiff base ligand HL (Scheme 2), derive from salicylaldehyde (SalH) and *N,N*-dimethyldipropylenetriamine, for exploration of coordination chemistry of cobalt in presence of different pseudohalide ions. Accordingly, we report herein, the synthesis and structures of four new cobalt complexes, $[Co(L)(N_3)_2]$ (**1**), $[Co(L)(NCS)_2]$ (**2**), $[Co(L)(Sal)]_2[Co(NCS)_2]$ **(3)** and $[Co(L)_2]_2[Co_{0.75}(NCS)_3]Cl_{0.5}$ (**4**). Remarkable coordination diversity influenced by both auxiliary anions and solvents used for the synthesis has been explored. The biomimetic catalytic activities of the synthesized complexes using *o*-aminophenol and two other substituted *o*-aminophenols as substrates have also been reported. Further emphasis was also given to explore the structure–function relationship along with the detailed mechanistic investigation, which is not yet explored for *o*-aminophenol derivatives.

2. Experimental section

2.1. Materials and physical measurements

Hexahydrated salts of cobalt(II) nitrate, cobalt(II) chloride, *o*-aminophenol (OAPH), salicylaldehyde, *N,N*-dimethyldipropylenetriamine, 2-amino-5-methylphenol, and 2-amino-4-methylphenol were purchased from commercial sources and used as received. Other chemicals and solvents were of reagent or analytical grade and used without further purification.

Caution! Metal complexes containing perchlorates and azide salts are potentially explosive. Although no problem was encountered in the present study, handling small amount of materials with great care is recommended.

Elemental analysis of carbon, hydrogen and nitrogen were carried out using a Perkin-Elmer 240C elemental analyser. UV-vis absorption spectra were measured in an Agilent Carry-60 diode array UV-vis spectrophotometer at room temperature with a 1-cm path-length quartz cell. IR spectroscopic data in the range 400–4000 cm^{-1} were collected in a PerkinElmer Spectrum Two FTIR spectrophotometer where samples prepared in KBr pellets. Electrochemical measurements of all complexes were conducted in a CH Instrument electrochemical workstation model CHI630E at a scan rate of 100–200 mVS^{-1}. The working electrode was platinum, polished with alumina solution, and air dried before each electrochemical run. The reference electrode was Ag/AgCl, with platinum as counter electrode. Tetrabutylammonium perchlorate was used as a supporting electrolyte. Electrospray ionization mass spectra (ESI-MS positive) were recorded in a Micromass Q-tof-Micro Quadruple mass spectrophotometer.

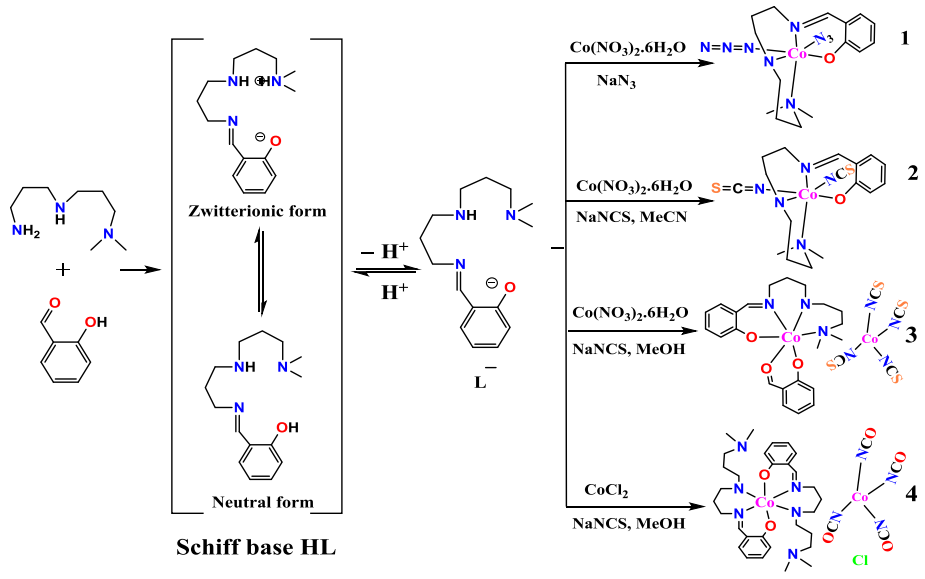

Scheme 2. Route to synthesis of the Schiff base and its cobalt complexes.

Table 1
Crystal data and structure refinement parameters of complexes **1** to **4.**

	1	2	3	4
Empirical formula	$C_{15}H_{24}CoN_9O$	$C_{17}H_{24}CoN_5OS_2$	$C_{24}H_{29}Co_{1.50}N_5O_3S_2$	$C_{63}H_{96}Co_{2.75}N_{15}O_{8.50}Cl_{0.50}$
Formula weight (g mol^{-1})	405.36	437.46	588.04	1379.32
Temperature (K)	293(2)	150(2)	293(2)	150(2)
Crystal system	Monoclinic	Monoclinic	Orthorhombic	Tetragonal
Space group	$P2_1/n$	$P2_1/c$	$Fdd2$	$P4/n$
a (Å)	9.5110(3)	10.301(10)	47.916(6)	26.8475(12)
b (Å)	19.6148(5)	12.479(5)	16.1405(9)	26.8475(12)
c (Å)	9.9662(3)	15.205(13)	13.6210(9)	9.7200(4)
α (°)	90	90	90	90
β (°)	103.627(2)	90.56(4)	90	90
γ (°)	90	90	90	90
volume ($Å^3$)	1806.92(9)	1954(3)	10534.3(17)	7006.1(5)
Z	4	4	16	4
D_{calc} (mg m^{-3})	1.490	1.487	1.483	1.312
μ (mm^{-1})	0.975	0.975	1.150	0.726
$F(0\,0\,0)$	848	912	4872	2935
θ Range (°)	2.08–26.22	2.679–30.706	1.70–28.19	2.23–26.42
Reflections collected	26,732	50,726	6847	72,904
Independent reflections (R_{int})	3606(0.0570)	6023(0.0452)	3990(0.0303)	14380(0.0540)
Observed reflections [I > 2σ(I)]	2761	5248	3641	10,596
Restraints/parameters	0/307	0/241	1/321	1/840
Goodness-of-fit on F^2	1.037	1.031	1.040	1.046
Final R indices [I > 2σ(I)]	R_1 = 0.0385	R_1 = 0.0247	R_1 = 0.0423	R_1 = 0.0643
	wR_2 = 0.0732	wR_2 = 0.0597	wR_2 = 0.0962	wR_2 = 0.1786
R indices (all data)	R_1 = 0.0584	R_1 = 0.0326	R_1 = 0.0476	R_1 = 0.0947
	wR_2 = 0.0796	wR_2 = 0.0652	wR_2 = 0.1000	wR_2 = 0.2023
Largest diff. peak/hole (e $Å^{-3}$)	0.254/ −0.240	0.393/–0.559	0.540/–0.462	1.620/–1.519

2.2. Synthesis of the Schiff-base ligand (HL)

Schiff base ligand (HL) was prepared by the reaction of *N,N*-dimethyldipropylenetriamine (1.0 mmol, 159 mg) and salicylaldehyde (1.0 mmol, 122 mg) in 20 ml of methanol (or acetonitrile) under refluxing condition for a period of 1 h. This *in situ* generated Schiff base ligand HL either in methanol or acetonitrile was used directly for the synthesis of the cobalt complexes as described below.

2.3. Synthesis of $[Co(L)(N_3)_2]$ (1)

Solid cobalt(II) nitrate hexahydrate (291 mg, 1.0 mmol) was added to a methanol solution of HL (1.0 mmol) with stirring at room temperature, leading to a dark-brown solution. A 5 ml 4:1 (v/v) methanol/water solution of sodium azide (130 mg, 2.0 mmol) was then added dropwise to the reaction mixture with constant stirring. The resulting solution was heated to reflux for about 30 min. It was then filtered and left at room temperature for slow evaporation. Block shape dark-brown crystals suitable for X-ray diffraction study were separated out from the filtrate after 3–4 days, which were collected by filtration and washed with methanol and were allowed to dry in air. Yield: 320 mg (79%). Anal. Calcd. for $C_{15}H_{24}CoN_9O$: C 44.45.21%, H 5.97%, N 31.10%. Found: C 44.29%, H 5.78%, N 31.03%. FTIR (KBr, cm^{-1}): $\nu(N_3)$ 2034 vs; ν(C═N) 1616 s.

2.4. Synthesis of $[Co(L)(NCS)_2]$ (2)

Complex **2** was synthesized from an acetonitrile/water (20:1, v/v) mixture following the same procedure as applied for the synthesis of complex **1.** The only difference is that an acetonitrile solution of NaSCN was used in place of NaN_3. Colour: Dark brown, Yield: 323 mg (74%). Anal. Calcd. for $C_{17}H_{24}CoN_5OS_2$: C 46.67%, H 5.53%, N 16.01%. Found: C 46.60%, H 5.45%, N 15.95%. FTIR (cm^{-1}, KBr): ν(NCS) 2063 s, ν(C═N) 1624 s.

2.5. Synthesis of $[Co(L)(sal)]_2[Co(NCS)_2]$ (3)

Complex **3** was synthesized from a methanol/water (20:1, v/v) mixture following same methodology as that employed for the synthesis of **1**, but methanolic solution of NaSCN was used in place of NaN_3. Colour: Dark brown, Yield: 343 mg (69%). Anal. Calcd. for $C_{48}H_{58}Co_3N_{10}O_6S_4$: C 49.02%, H 4.97%, N 11.91%. Found: C 48.96%, H 4.84%, N 11.87%. FTIR (cm^{-1}, KBr): ν(NCS) 2065 s, ν(C═N) 1625 s.

2.6. Synthesis of complex $[Co(L)_2]_2[Co_{0.5}(NCS)_2][Co_{0.25}(NCS)]Cl_{0.5}$ (4)

Similar methodology as that applied for the synthesis of **1** was adopted for the preparation of **4** from a methanol/water (20:1, v/v) mixture, but using chemicals $CoCl_2{\cdot}6H_2O$ and NaNCO. Colour: Dark brown, Yield: 343 mg (69%). Anal. Calcd. for $C_{63}H_{96}Co_{2.75}N_{15}O_{8.50}Cl_{0.5}$: C 54.86%, H 7.02%, N 15.23%. Found: C 54.79%, H 6.99%, N 15.27%. FTIR (cm^{-1}, KBr): ν(NCO) 2215 s, ν(C═N) 1628 s.

2.7. X-ray diffraction study

X-ray diffraction data of **1–4** were collected on a Bruker SMART APEX-II CCD diffractometer using graphite monochromated Mo Kα radiation (λ = 0.71073 Å). Data processing, structure solution, and refinement were performed using Bruker Apex-II suite program. The highly redundant data sets were reduced using SAINT-plus and corrected for Lorentz and polarization effects. Absorption corrections were applied using SADABS [42] supplied by Bruker. The structures were solved using the direct method and refined by the successive full-matrix least-squares cycles on F^2 using SHELXL-v.2014 [43]. All nonhydrogen atoms were refined with anisotropic displacement parameters. Hydrogen atoms were placed in calculated positions and refined as riding atoms with their fixed isotropic thermal parameters which are tied 1.2 times or 1.5 times (for methyl group) with their parent atoms. The crystal structures of all complexes were generated using MERCURY-3.10.1 software. Details of X-ray crystallographic data collection and structure refinements are summarized in Table 1.

2.8. Catalytic oxidation of o-aminophenols

The catalytic oxidation of substrate *o*-aminophenol was studied by the reaction of the substrate (1.0×10^{-2} M) in presence of catalytic

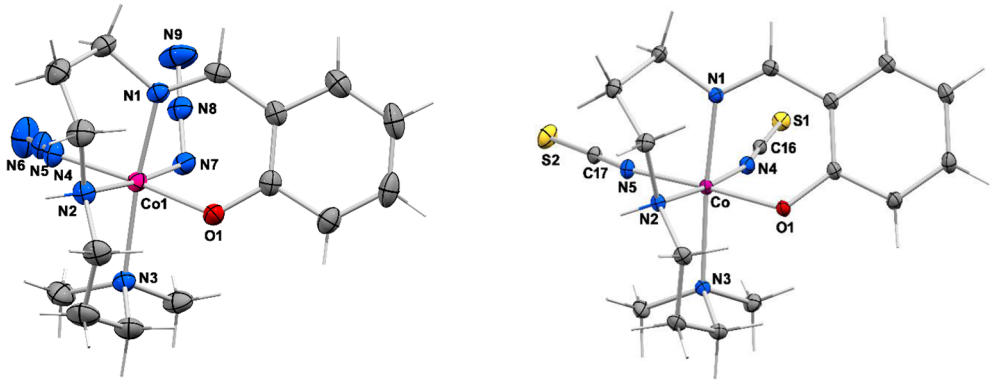

Fig. 1. The molecular structures of **1** and **2** with selected atom numbering schemes. Thermal ellipsoids are drawn at 30% probability.

amount of the complexes (5×10^{-5} M) in air saturated methanol at room temperature. The aerobic oxidation of OAPH catalysed by **1–4** was investigated UV-vis spectrophotometrically by monitoring increase of the characteristic absorbance band of 2-aminophenoxazin-3-one as a function of time at 435 nm. To evaluate various kinetic parameters, the kinetic measurements were conducted for all complexes where a fixed amount of the complex were subjected to react with variable concentrations of the substrate maintaining the pseudo-first-order condition. All the kinetic measurements were carried out for the period of 10 min and the initial rate of the reaction was determined by the linear regression from slope of the absorbance verses time plot. Similar methodology was applied to check the catalytic oxidation of the substituted *o*-aminophenols using **1** and **2** as catalysts

3. Results and discussion

3.1. Syntheses and general characterizations

The Schiff base (HL) ligand used in the present study was prepared by the reaction of salicylaldehyde and *N,N*-dimethyldipropylenetriamine in a 1:1 M ratio in methanol or acetonitrile under refluxing condition (Scheme 2). This *in situ* generated ligand thereafter by the reaction with cobalt(II) nitrate hexahydrate in the presence of pseudohalides in a 1:1:2 M ratio produced different compounds of compositions $[Co(L)(N_3)_2]$ (**1**), $[Co(L)(NCS)_2]$ (**2**) and $[Co(L)(Sal)]_2[Co(NCS)_4]$ (**3**), in reasonable yields. Furthermore, a mixture of cobalt(II) chloride and the Schiff base in presence of NaNCO yielded $[Co(L)_2]_2[Co_{0.75}(NCS)_3]Cl_{0.5}$ (**4**) as only the isolable product. It is noted that when thiocyanate auxiliary ion was used, the resulting products are highly dependent on the solvents used for the syntheses, but no effect has been observed on the stoichiometric ratios of the reactants. When the synthesis was carried out in an acetonitrile/water solvent mixture, it produced only isolable product **2**, whereas identical reaction in a methanol/water solvent using the same reactants resulted only isolable product **3** in reasonable yield. These diverse results clearly justify that the reaction condition is very much crucial for the formation of these complexes. Further, isolation of different products from the same reactants but from different solvents clearly indicates that both of them are thermodynamic products, and both formation and stability of them are dependent on the solvents used for their syntheses, that governs the identity of the species that crystallizes from a particular solvent. However, as found in the similar ligand systems, the starting cobalt(II) metal centre in each case is air-oxidized to cobalt(III), especially when it is coordinated to the Schiff base ligand. The solubility of all complexes is more or less remain same and they are soluble in the most common organic solvents like methanol, acetonitrile and DMF. Furthermore, the purity of bulk samples was verified by the elemental analyses, which is matched well with the X-ray crystallographic results.

IR spectra of all complexes display the characteristic stretching vibrations of the azomethine bond of the Schiff base ligand coordinated to the metal centre in the range 1615–1626 cm^{-1}. In addition, strong bands appeared at 2032 and 2215 cm^{-1} in the IR spectra of **1** and **4** can be assigned to the stretching vibration of coordinated azide and cyanate ions, respectively [41a,44]. Similarly, the strong bands observed at 2087–2125 and 2057 cm^{-1} in the IR spectra of **2** and **3**, respectively, are attributed to stretching vibration of the coordinated thiocyanate ions, implying coordination of the NCS^- ion through the nitrogen end [41a,44]. Significantly lower stretching frequency of the thiocyanate ion in **3** is probably due to greater π acceptor ability of thiocyanate from cobalt(II) centre compared to its π acceptor ability from cobalt(III) centre in **2**.

3.2. Structural descriptions

Crystal structures of the reported complexes were determined by the single crystal X-ray diffraction method. The crystal structures of **1** and **2** are presented in Fig. 1, while Fig. 2 displays the solid-state structures of **3** and **4**. Selected bond distances around the metal coordination sphere for all complexes are given in Table 1. Both **1** and **2** crystallize in the monoclinic unit cell but with different space groups $P2_1/n$ and $P2_1/c$, respectively. Asymmetric units of both **1** and **2** consist of full set of a neutral complex molecule. In both complexes, cobalt(III) centres reveal a distorted octahedral N_5O coordination environment in which the metal centre is coordinated with phenolate oxygen atom, imine nitrogen atom, secondary amine nitrogen and tertiary amine nitrogen of the monoanionic Schiff base ligand and two remaining coordination sites are occupied by two nitrogen atoms from two terminal azide (in **1**) and thiocyanate (in **2**) ions. X-ray crystal structure determination shows slight deviation of *cisoid* (83.62(7)–93.45(8)°) and *transoid* (174.72(8)–176.97(4)°) angles from the ideal values which justifies the slightly distorted octahedral geometry around the metal centre in these complexes. The triamine part of the Schiff base ligand constitutes one meridional position, while other meridional position is occupied by two nitrogen atoms of pseudohalides together with the phenolate-O atom of the Schiff base. In both complexes, the Co–O(phenolate) distances of the tetradentate ligand and Co–N(pseudohalide) distances are in the range1.8654(17)–1.8770(15) and 1.9094(19)–1.953(2) Å, respectively, and are in accordance with the bond lengths as found in reported low-spin octahedral cobalt(III) complexes with similar coordination environment [41b,41c,45–54]. The Co–N bond lengths of imine, secondary and tertiary amines span in the range 1.922(2)–1.9223(19), 1.983(2)–2.008(2) and 2.097(2)–2.1082(19) Å, respectively in both complexes. Here, the secondary amine bonds are somewhat longer than the imine moieties in both complexes (see Table 1), which resemble with their standard states of hybridization. Moreover, the bond length of tertiary amine is significantly longer than the secondary amine group which is again consistent with the reduced Lewis basicity of tertiary amine, leading to the weaker binding propensity to the metal centre

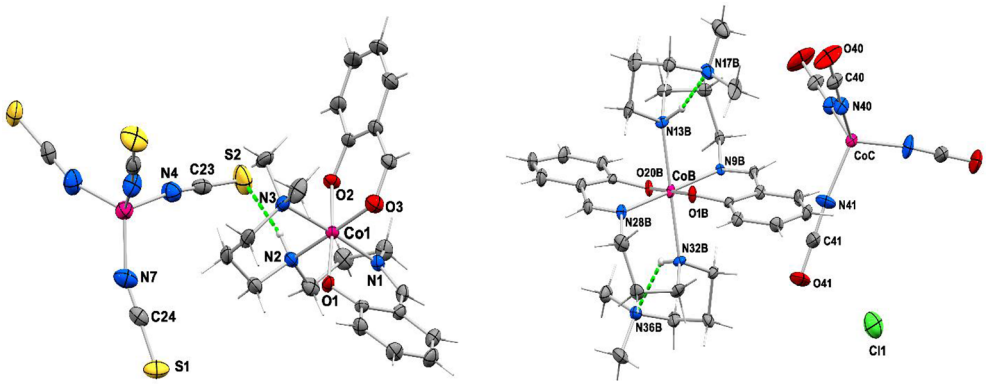

Fig. 2. The partial crystal structures of **3** and **4** displaying both complex cation and complex anions with selected atom labelling scheme. Ellipsoids are drawn in 30% probability.

[41]. The N–N bond distances of the azide ions ranging from 1.152(3)–1.199(3) Å indicate the coordination through the anionic terminal of azide ion [41b,41c,52–54]. Similarly, the bond distances associated with thiocyanate ion in complex **2** are typical for coordination through the nitrogen end [41b,41c,52–54]. The solid-state structure of **1** is stabilized by the intermolecular N—H···N hydrogen bonding interaction involving secondary amine and one of the terminal nitrogen atom of coordinated azide ion with N···O distance of 3.238(3) Å between the adjacent molecules (Fig. S1). Stability in the solid state is further reinforced by the multiple C—H···π interactions between the neighbouring molecules in **1** as depicted in the figure. Similar pattern of hydrogen bonding interaction is also present in the solid state structure of **2** in which the secondary amine forms hydrogen bond with the sulphur atom of coordinated thiocyanate ion from a neighbouring molecule with N···S distance of 3.428(3) Å. Apart from that the C—H···π interaction involving two adjacent molecules provides additional stability of compound **2** in the solid state (Fig. S2).

X-ray diffraction study reveals that complex **3** crystalizes in the orthorhombic *Fdd*2 space group, whereas complex **4** crystalizes in the tetragonal *P*4/*n* space group. The asymmetric unit of **3** consists of a complex cation of composition $[Co(L)(Sal)]^+$ on a general position and a complex anion $Co(NCS)_4^{2-}$ on a two-fold axis of symmetry. The geometry of the metal centre of complex cation $[Co(L)(Sal)]^+$ is pseudo-octahedral with N_3O_3 coordination environment, comprising with N_3O donor set of the deprotonated Schiff base ligand and two O-atoms from deprotonated salicylaldehyde molecule. The Schiff base ligand binds the metal centre exactly in similar fashion as found in the crystal structures of **1** and **2**. Therefore, the Co–N bond distances of *N*-atoms of imine, secondary and tertiary amines found to be 1.935(4), 2.017(4) and 2.105(4) Å, respectively, in **3** are similar to bond distances observed in **1** and **2**. Again, they are comparable to low-spin octahedral cobalt(III) complexes with similar coordination environments [41b,41c,45–54]. The Co–O (phenolate) and Co–O (salicylaldehyde) bond distances are 1.880(3) and, 1.889(3) and 1.907(4) Å, respectively, typical for cobalt(III) coordination chemistry. In complex anion $Co(NCS)_4^{2-}$, the cobalt(II) centre has distorted tetrahedral geometry with the Co–N bond lengths of 1.934(5) and 1.937(5) Å and the N–Co–N bond angles ranging from 105.7(2)° to 116.3(4)° [55–58].

The asymmetric unit of complex **4** includes two crystallographically independent complex cations of composition $[Co(L)_2]^+$ on general positions, two distinct $Co(NCO)_4^{2-}$ complex anions either siting on a two-fold axis of symmetry or on a four-fold axis of symmetry along with a chloride ion on a four-fold axis of symmetry. The structures of both crystallographically independent complex cations are eventually similar in which the metal centre has distorted octahedral geometry with N_4O_2 coordination environments. In this system, the Schiff base ligands coordinate the metal centre facially using N_2O donor sites of the ligand, but electroneutrality of the systems demands that the ligand is monoanionic in **4**. Participation of free tertiary amine group in the intramolecular hydrogen bonding as an acceptor with the secondary amine group of the same ligand (see Fig. 2, right) further ensures the monoanionic state of the coordinated ligand. The Co–O(phenolate), Co–N(imine) and Co–N(secondary amine) bond lengths are in the range 1.952(4)–1.938(5), 2.016(6)–2.040(5) and 1.893(4)–1.902(4) Å, respectively for complex **4**. As usual, cobalt(II) centre in the complex anions is tetrahedrally bonded with nitrogen atoms of four cyanate ions [55–58] with bond angles (N–Co–N) varying in the range 108.0(3)–112.0(5)°.

3.3. Electrochemical studies

The electrochemical studies of all complexes carried out in methanol, the same medium used for the catalytic experiments, at a scan rate of 100 mV/s with respect to a Ag/AgCl electrode at room temperature. Representative cyclic voltammograms of **2** and **3** are depicted in Fig. 3, while the electrochemical data of all complexes are assembled in Table 2. In the negative potential region, the complexes exhibit an irreversible reduction wave varying in a narrow range of −0.65–−0.86 V, that is consistent with the diverse coordination environments of the metal centre in these complexes. In the positive potential region, only complexes **3** and **4** exhibit an irreversible oxidative response at 0.90 V (for **3**) and 0.93 V (for **4**). This oxidative response is due to the presence of complex anion of general formula $[CoX_4]^{2-}$

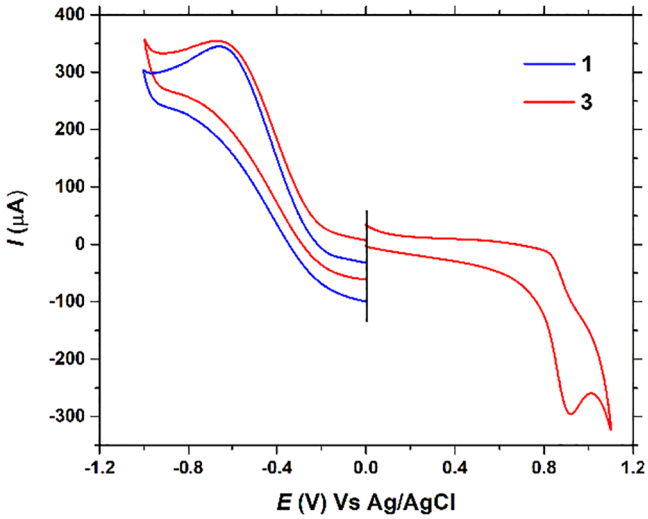

Fig. 3. Cyclic voltammograms of **1** and **3** in methanol using a platinum working electrode in the presence of tetrabutylammonium perchlorate as a supporting electrolyte at room temperature with scan rate 100 mV s^{-1}.

Table 2
Selected bond distances (Å) for complexes **1–4**.

Bond	1	2	3	4
Co(III)–N(imine)	1.922(2)	1.9223(19)	1.935(4)	1.952(4) 1.938(5)
Co(III)–N(secondary amine)	1.983(2)	2.008(2)	2.017(3)	2.016(6) 2.040(5)
Co(III)–N(tertiary amine)	2.097(2)	2.1082(19)	2.105(4)	–
Co(III)–O(phenolate)	1.8654(17)	1.8770(15)	1.880(3)	1.893(4) 1.902(4)
Co(III)–O(free aldehyde)	–	–	1.889(3) 1.907(4)	–
Co(III)–N(pseudohalide)	1.9098(19) 1.9094(19)	1.947(2) 1.953(2)	–	–
Co(II)–N(pseudohalide)	–	–	1.934(5) 1.937(5)	1.983(6) 1.952(6) 1.941(6)

(X = SCN for **3**, NCO for **4**) where the oxidation of cobalt(II) to cobalt (III) takes place.

3.4. Oxidation studies with substituted aminophenols

Oxidation of *o*-aminophenol (OAPH) by molecular dioxygen in presence of catalytic amount of the complexes in aerobic condition was studied using UV–vis spectrophotometer at room temperature. For that, 5.0×10^{-5} M methanolic solution of the complexes were allowed to react with a 1.0×10^{-2} M solution of OAPH. The spectral change due to formation of 2-aminophenoxazinone (Phx-1) was recorded UV–vis spectrophotometrically. Spectral profiles for aerobic oxidation of OAPH catalyzed by **1** and **2** for a period of 1 h (at 5 min interval) are depicted in Fig. 4, whereas Fig. S3 represents the oxidation of OAPH by **3** and **4** respectively. The gradual increase of peak intensity at *ca.* 435 nm implies the formation of Phx-1 as a function of time [59]. The spectral profile further suggests that complex **1** and **2** are efficient catalysts for the oxidation of OAPH, while **3** and **4** are less reactive. Moreover, the detailed kinetic study is performed to get insight into the catalytic efficiency of these complexes. For that 1.0×10^{-5} M solutions of the complexes were reacted with excess substrate at the pseudo-first-order condition and initial rates were evaluated. Initial rate versus concentration of the substrate plots for oxidation of OAPH catalyzed by **1–4** show a typical rate saturation kinetics (Fig. 5). These results suggest that an intermediate complex-substrate aggregate is formed in a pre-equilibrium stage followed by the irreversible redox transformation of the intermediate in the rate determining step of the catalytic cycle. Michaelis–Menten approach was applied for evaluation of kinetic parameters V_{max}, K_M, and K_{cat} (Table 3) for such rate saturation kinetics. The turnover numbers (TON) of the catalysts were then

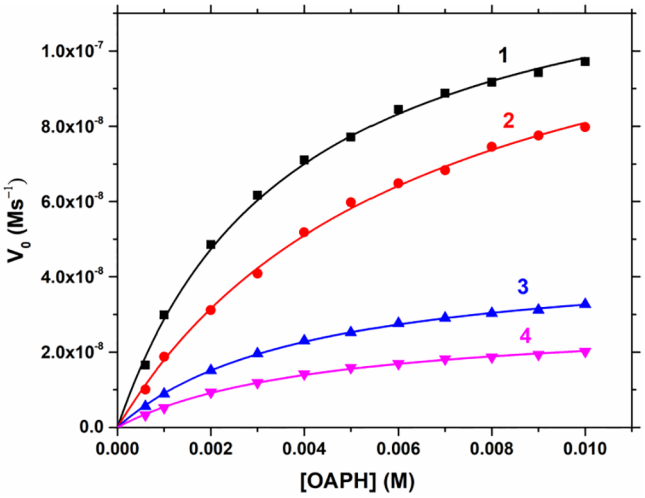

Fig. 5. Initial rate versus substrate concentration plot for the oxidation of OAPH in dioxygen-saturated methanol catalysed by **1–4** at room temperature. Symbols and solid lines represent the experimental and simulated profiles, respectively.

Table 3
Cyclic voltammetric data for **1–4** at room temperature.

Complex	Reduction (Co^{III}/Co^{II})	Oxidation (Co^{II}/Co^{III})
1	–0.65 V	–
2	–0.68 V	–
3	–0.65 V	0.90 V
4	–0.86 V	0.92 V

calculated by dividing the value of V_{max} by the concentration of catalyst used and are reported to be 47.36, 47.60, 16.46 and 10.34 h^{-1} for **1–4**, respectively.

A good numbers of model catalysts have been reported mimicking the function of phenoxazinone synthase to gain clear idea about the possible mechanism and to check efficiency of the synthetic analogues. Comparing the present results with literature data, it is clear that although **3** and **4** are less reactive but **1** and **2** are efficient catalysts for aerial oxidation of *o*-aminophenol. It is to be further noted that the catalytic oxidation of some substituted *o*-aminophenols in terms of isolations and characterizations of their oxidised products were available in the literature, but the detailed kinetic studies were not reported. Therefore, in this present study we examined the detailed catalytic activity using two substituted *o*-aminophenols, namely 2-amino-5-methylphenol (5MeOAP) and 2-amino-5-methylphenol (4MeOAP) to get

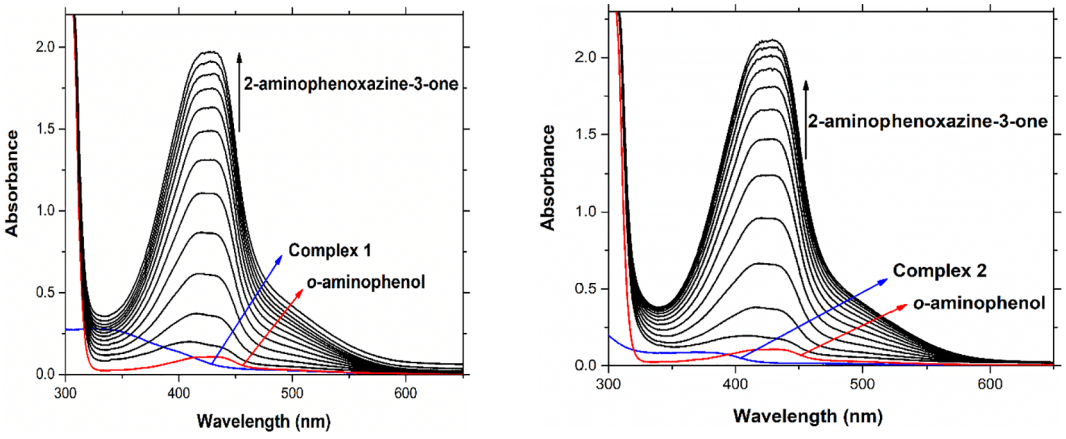

Fig. 4. Increase in absorption band for the oxidation of *o*-aminophenol (1.0×10^{-2} M) catalysed by **1** and **2** (5.0×10^{-5} M) in dioxygen-saturated methanol.

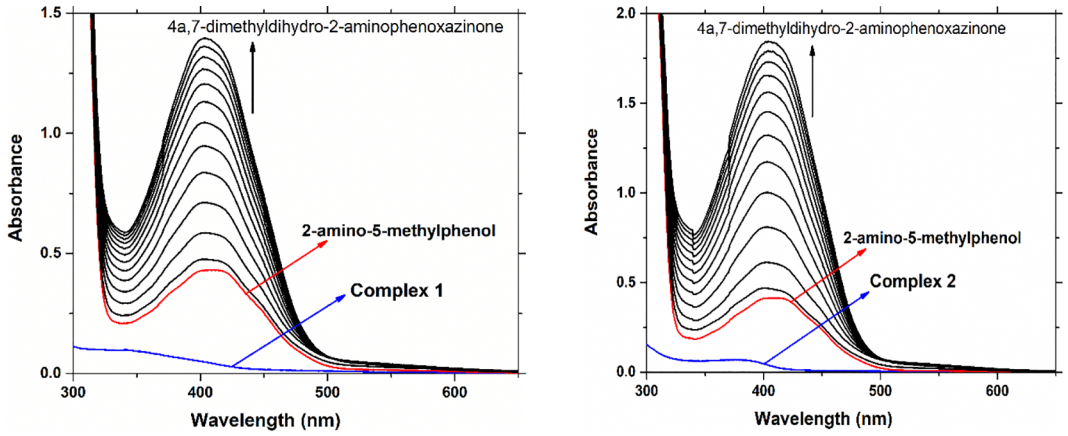

Fig. 6. Time resolve spectral profile showing growth of 4a,7-dimethyldihydro-2-aminophenoxazinone at 405 nm upon addition of 5.0×10^{-3} M and 1.0×10^{-2} M 2-amino-5-methylphenol to a solution containing 1 (1×10^{-5} M)(left) and 2 (5×10^{-5} M)(right) respectively in dioxygen-saturated methanol.

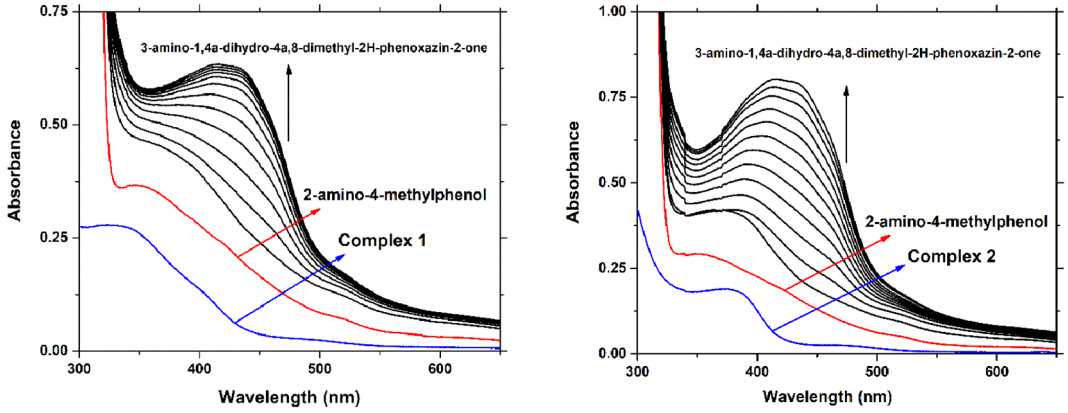

Fig. 7. Spectral scan showing oxidation of 2-amino-4-methylphenol (1.0×10^{-2} M) catalysed by 1 and 2 (5×10^{-5} M) in dioxygen-saturated methanol.

further insights into the reactive intermediates and the mechanistic details of the catalytic reactions and finally to establish the structure-reactivity correlation of the catalysts. For that the reaction kinetics of the formation of 2-amino-4,4a-dihydro-4a-7-dimethyl-3*H*-phenoxazine-3-one (Phx-2), and 3-amino-1,4a-dihydro-4a,8-dimethyl-2H-phenoxazin-2-one (Phx-3) were carried out for a period of 10 min using the most reactive compounds **1** and **2** as depicted in Figs. 6 and 7, respectively. Similar kinetic profiles as found for the oxidation of *o*-aminophenol are also obtained for the substituted *o*-aminophenols (Fig. 8), indicating that all these substrates oxidations follow similar catalytic pathway. Detailed kinetic analysis further gives us the values of various kinetic parameters V_{max}, K_M, and K_{cat} which along with turnover numbers are assembled in Table 4.

3.5. Mechanistic pathway and mass spectrometry

Catalytic efficiency of the oxidase metalloenzymes and their synthetic analogues depends on several factors among which the electronic environment around the metal centers and available coordination sites for substrate binding are the most important factors. In present systems, although the reduction potentials of the cobalt(III) centres are comparable, the facile substrate binding by the replacement of coordinated pseudohalides (azide ions in **1** and thiocyanate ions in **2**) from the metal centres, leading to the formation of stable complex-substrate intermediates, are responsible for higher catalytic activity of **1** and **2** than **3** and **4**. Kinetic data further show that the catalytic oxidation of methyl substituted *o*-aminophenols is rather favourable than that of *o*-aminophenol itself, which is consistent with the electronic structures of the substrates where the methyl substitution in the benzene ring facilitates the oxidation of methyl-substituted o-aminophenols. Interestingly, both the rate saturation kinetics and mass spectrometry (*vide infra*) clearly suggest that the methyl substitution does not inhibit formation of the complex-substrate intermediate, but the final two-electrons oxidation step was blocked by methyl substitution, leading to the formation of dihydro-aminophenoxazinone chromophore instead of aminophenoxazinone chromophore which is the final oxidation product of *o*-aminophenol itself.

The mass spectrometry is quite helpful as it proves significant information regarding the product and intermediate species from which one can schematically represent the most probable mechanistic pathway of the catalytic action. For that, the electrospray ionization mass spectra of a reactive compound **2** both in absence and presence of 2-amino-5-methylphenol (20 equivalents) in methanol were recorded and are depicted in Figs S4 and S5, respectively. The mass spectrum of compound **2** is clean enough and it consists of only one major peak at m/z = 321.10 which is nothing but the peak of complex cation without thiocyanate ions of formula $[Co(L)]^+$ (calcd. m/z = 321.13). Interestingly, when mass spectrum of **2** was recorded in presence of 20 equivalents of 2-amino-5-methylphenol, the base peak is shifted at m/z = 243.10, which is matched well with the protonated species of the product 2-amino-4,4a-dihydro-4a-7-dimethyl-3*H*-phenoxazine-3-one (calcd. m/z = 243.11). The original peak of the complex cation at m/z = 321.10 converted to a minor component in presence of the substrate. Moreover, a minor peak at m/z = 124.11 (calcd. m/z = 124.08)

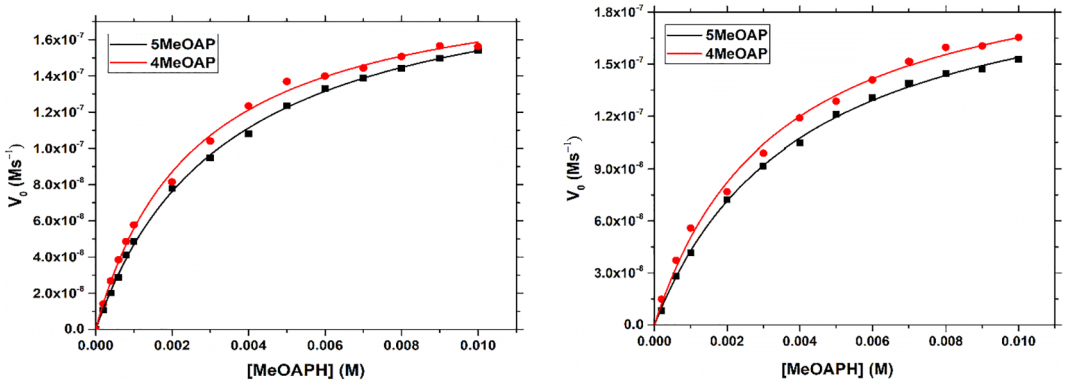

Fig. 8. Initial rate versus substrate concentration plot for the oxidation of OAPH in dioxygen-saturated methanol catalysed by **2** and **3** at room temperature. Symbols and solid lines represent the experimental and simulated profiles, respectively.

was found in the mass spectrum, related to the protonated species of the substrate itself. The appearance of a major peak at *m/z* 443.15 is the most interesting one as it matches with a complex-substrate intermediate species of composition $[Co^{III}(L)(2\text{-amino-5-methylphenolate})]^+$ (calcd. *m/z* = 443.19). These observations clearly support the ease of formation of the stable complex-substrate aggregates, exploiting the stronger chelating ability of *o*-aminophenolate ions by substituting the terminal pseudohalide ions.

Now we are at right position to tempt a well acceptable plausible mechanism compiling the preceding information. Both the mass spectrometry and kinetic data clearly establish that the catalytic cycle for the aerobic oxidation of *o*-aminophenol catalysed by **1** and **2** starts with the formation of a stable complex-substrate aggregate through the replacement of coordinated pseudohalides by *o*-aminophenolate ion. This complex-substrate intermediate produces *o*-aminophenolate radical through the inner sphere electron transfer from *o*-amionophenolate to the cobalt(III) centre in the rate determining step. Facile oxidation upon methyl substitution at benzene ring, leading to the higher turnover rates, further suggests that the aminophenolate oxidation is the rate determining step. Being unstable the OAP radical thereafter is oxidised to *o*-benzoquinone monoamine (BQMI) in several ways including the disproportionation of the OAP radical itself. The intermediate (BQMI) ultimately produces 2-aminophenoxazin-3-one through the couples of oxidative dehydrogenations intermediate steps as shown in Scheme 3. Similar mechanistic pathway is also applicable for catalytic oxidation of 2-amino-5-methylphenol or 2-amino-4-methylphenol in which methyl substitution does not inhibit the formation of a stable complex-substrate intermediate as evidenced by the mass spectrometry. Although the methyl substitution does not inhibit the coupling of two aminophenols, but the final oxidative dehydrogenation step was blocked by the methyl substitution, leading to the formation of dihydro-phenoxazinone chromophore (2-amino-4,4a-dihydro-4a-7-dimethyl-3*H*-phenoxazine-3-one for 2-amino-5-methylphenol and 3-amino-1,4a-dihydro-4a,8-dimethyl-2H-phenoxazin-2-one for 2-amino-4-methylphenol) instead of phenoxazinone chromophore as found for the oxidation of *o*-aminophenol itself (see Scheme 3).

4. Conclusions

Four cobalt complexes were synthesized by the reaction of a new tetradentate Schiff base ligand, derived from *N,N*-dimethyldipropylenetriamine and salicylaldehyde, and cobalt(II) salts in presence of different pseudohalide ions. X-ray crystallographic studies reveal that both counter ions and solvents have significant influence on the structural diversities of the resulting complexes. All these complexes were found active catalysts for the aerobic oxidation of different o-aminophenols. Among them, **1** and **2** are highly reactive as in these systems substitutionally labile metal-bound pseudohalide ions are available for substrate binding. The detailed kinetic studies of the aerobic oxidation of two substituted o-aminophenols, namely 2-amino-5-methylphenol and 2-amino-4-methylphenol, were further examined using highly reactive catalysts **1** and **2**. Remarkably, the catalytic oxidation of methyl substituted *o*-aminophenols is much favourable than the parent *o*-aminophenol which is the consequence of electron donating effect of methyl substitution. Mass spectrometry reveals that the methyl substitution does not inhibit the formation of a stable complex-substrate intermediate in the catalytic cycle, but the final oxidative dehydrogenation step is inhibited in the presence of methyl group, leading to the formation of dihydro-phenoxazinone chromophore instead of phenoxazinone chromophore.

Acknowledgements

A. P. also gratefully acknowledges the financial support of this work by the University Grant Commission, India (Sanction no. F. PSW-229/15-16(REO)). Panskura Banamali College acknowledges the grants re-

Table 4
Kinetic parameters of oxidation of *o*-aminophenols catalysed by **1**–**4**.

Substrate	Catalyst	V_{max} (Ms^{-1})	K_M (M)	k_{cat} (h^{-1})
OAPH	**1**	$(1.31 \pm 0.02) \times 10^{-7}$	$(3.46 \pm 0.13) \times 10^{-3}$	47.36
	2	$(1.32 \pm 0.03) \times 10^{-7}$	$(6.36 \pm 0.35) \times 10^{-3}$	47.60
	3	$(4.57 \pm 0.04) \times 10^{-8}$	$(4.04 \pm 0.10) \times 10^{-3}$	16.46
	4	$(2.87 \pm 0.04) \times 10^{-8}$	$(4.21 \pm 0.15) \times 10^{-3}$	10.34
2-amino-5-methylphenol	**1**	$(2.07 \pm 0.02) \times 10^{-7}$	$(3.43 \pm 0.11) \times 10^{-3}$	74.38
	2	$(2.16 \pm 0.03) \times 10^{-7}$	$(4.06 \pm 0.13) \times 10^{-3}$	77.85
2-amino-4-methylphenol	**1**	$(2.00 \pm 0.03) \times 10^{-7}$	$(2.59 \pm 0.12) \times 10^{-3}$	71.94
	2	$(2.21 \pm 0.06) \times 10^{-7}$	$(3.39 \pm 0.22) \times 10^{-3}$	79.66

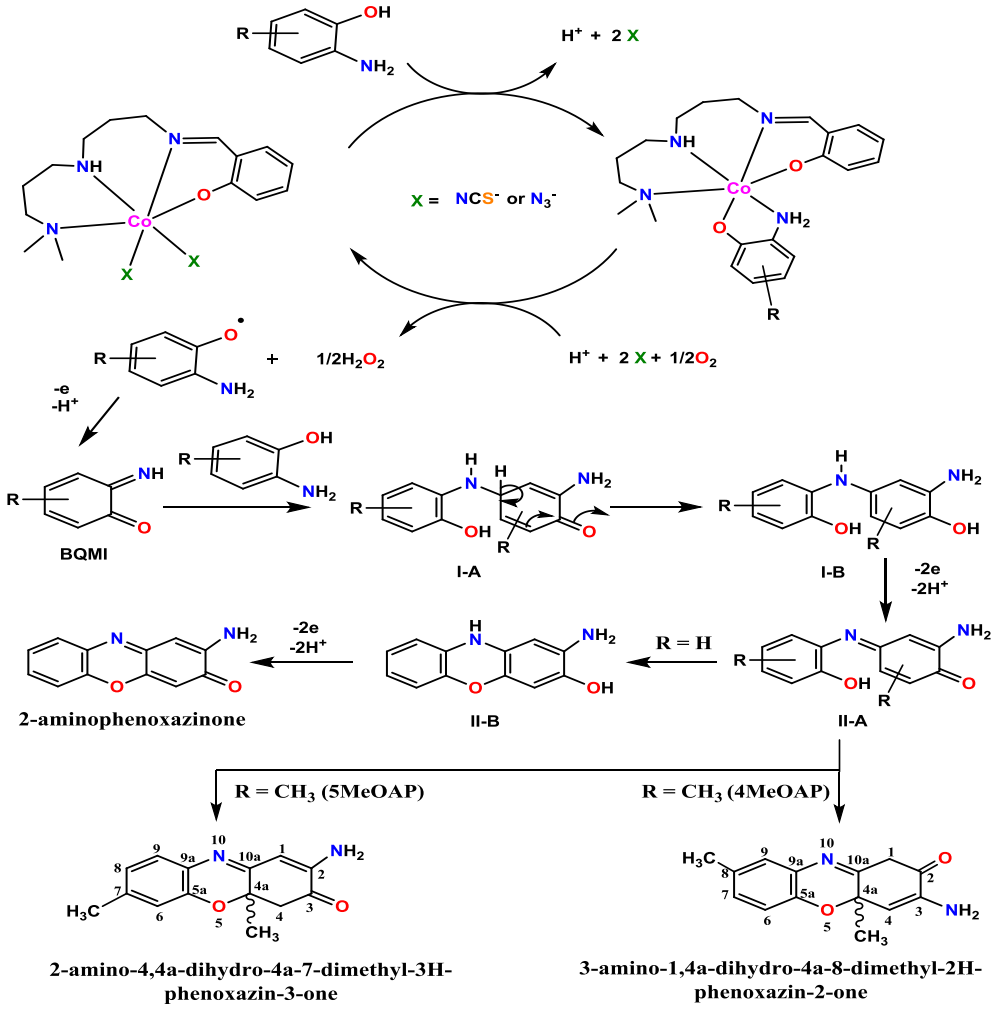

Scheme 3. Plausible mechanistic pathway for the aerobic oxidation of *o*-aminophenols catalysed by **1** and **2**.

ceived from Department of Science and Technology (DST), Govt. of India through FIST program (SR-FIST-Col/295 dated 18/11/2015). The authors thank Jadavpur University, Kolkata, India, for providing the Mass spectrometry facility.

Appendix A. Supplementary data

The electronic supporting information file contain Figures. S1–S5. CCDC 1888079–1888082 contain the supplementary crystallographic data for **1–4**, respectively. Supplementary data to this article can be found online at https://doi.org/10.1016/j.ica.2019.03.017.

References

[1] H. Naeimi, Z.S. Nazifi, S.M. Amininezhad, M. Amouheidari, J. Antibiot. 66 (2013) 687.
[2] M. Hajrezaie, M. Paydar, C.Y. Looi, S.Z. Moghadamtousi, P. Hassandarvish, M.S. Salga, H. Karimian, K. Shams, M. Zahedifard, N.A. Majid, H.M. Ali, M.A. Abdulla, Sci. Rep. 5 (2015) 9097.
[3] T. Mukherjee, J.C. Pessoa, A. Kumar, A.R. Sarkar, Dalton Trans. 42 (2013) 2594.
[4] A. Lehwess-Litzmann, P. Neumann, C. Parthier, S. Lüdtke, R. Golbik, R. Ficner, K. Tittmann, Nat. Chem. Biol. 7 (2011) 678.
[5] P. Adaeo, M.L. Kuznetsov, S. Barroso, A.M. Martins, F. Avecilla, J.C. Pessoa, Inorg. Chem. 51 (2012) 11430.
[6] D. Gong, B. Wang, X. Jia, X. Zhang, Dalton Trans. 43 (2014) 4169.
[7] P. Das, W. Linert, Coord. Chem. Rev. 311 (2016) 1.
[8] W. Al Zoubi, Y.G. Ko, J. Organomet. Chem. 822 (2016) 173.
[9] A.M. Abu-Dief, I.M.A. Mohamed, J. Basic Appl. Sci. 4 (2015) 119.
[10] S.H. Li, F.R. Chen, Y.F. Zhou, J.N. Wang, H. Zhang, J.G. Xu, Chem. Commun. (2009) 4179.
[11] S.A. Lee, G.R. You, Y.W. Choi, H.Y. Jo, A.R. Kim, I. Noh, S.J. Kim, Y. Kim, C. Kim, Dalton Trans. 43 (2014) 6650.
[12] A. Ganguly, B.K. Paul, S. Ghosh, S. Kar, N. Guchhait, Analyst 138 (2013) 6532.
[13] W. Al Zoubi, N. Al Mohanna, Spectrochim. Acta Part A: Mol. Biomol.Spectrosc. 132 (2014) 854.
[14] P.A. Vigato, S. Tamburini, Coord. Chem. Rev. 248 (2004) 1717.
[15] R.M. Clarke, T. Storr, Dalton Trans. 43 (2014) 9380.
[16] T. Horvath, J. Kaizer, G. Speier, J. Mol. Catal. A Chem. 215 (2004) 9.
[17] L.I. Simandi, M. Tatiana, Z. May, G. Besenyei, Coord. Chem. Rev. 245 (2003) 85.
[18] T.M. Simandi, L.I. Simandi, M. Gyor, A. Rockenbauer, A. Gomory, Dalton Trans. (2004) 1056.
[19] C.E. Barry, P.G. Nayar, T.P. Begley, J. Am. Chem. Soc. 110 (1988) 3333.
[20] E. Frei, Cancer Chemother. Rep. 58 (1974) 49.
[21] U. Hollstein, Chem. Rev. 74 (1974) 625.
[22] Alex W. Smith, Ana Camara-Artigas, Meitian Wang, James P. Allen, Wilson A. Francisco, Biochemistry 45 (14) (2006) 4378.
[23] M. Le Roes-Hill, C. Goodwin, S. Burton, Trend. Biotechnol. 27 (4) (2009) 248.
[24] S.K. Dey, A. Mukherjee, Coord. Chem. Rev. 310 (2016) 80.
[25] R. Muthusami, M. Moorthy, K. Irena, A. Govindaraj, C. Manickam, R. Rangappan, New J. Chem. 42 (23) (2018) 18608.
[26] B. Chowdhury, B. Bhowmik, A. Sahu, M. Joshi, S. Paul, A.R. Choudhury, B. Biswas, J. Chem Sci. 130 (12) (2018) 161.
[27] M. Mahato, K. Van Hecke, H.P. Nayek, Appl. Organomet. Chem. 32 (5) (2018) 4336.
[28] A. Das, K. Bhattacharya, L.K. Das, S. Giri, A. Ghosh, Dalton trans. 47 (28) (2018) 9385.
[29] K. Ghosh, A. Banerjee, A. Bauzá, A. Frontera, S. Chattopadhyay, RSC Adv. 8 (49) (2018) 28216.
[30] A. Panja, A. Frontera, Eur. J. Inorg. Chem. 7 (2018) 924.
[31] A. Panja, N.C. Jana, M. Patra, P. Brandao, C.E. Moore, D.M. Eichhorn, A. Frontera, J. Mol. Catal. A Chem. 412 (2016) 56.
[32] A. Panja, Polyhedron 79 (2014) 258.
[33] A. Panja, RSC Adv. 4 (2014) 37085.
[34] S. Shimizu, M. Suzuki, A. Tomoda, S. Arai, H. Taguchi, T. Hanawa, S. Kamiya, Tohoku J. Exp. Med. 203 (2004) 47.
[35] D.J. Kosman, Metallomics 10 (3) (2018) 370.

[36] L. Cortes, B.R. Roberts, A.G. Wedd, Z. Xiao, Inorg. chem. 56 (9) (2017) 5275.
[37] A. Panja, Polyhedron 80 (2014) 81.
[38] A. Panja, M. Shyamal, A. Saha, T.K. Mandal, Dalton Trans. 43 (2014) 5443.
[39] A.K. Ghosh, C.S. Purohit, R. Ghosh, Polyhedron 155 (2018) 194.
[40] A. Company, L. Gomez, R. Mas-Balleste, I.V. Korendovych, X. Ribas, A. Poater, T. Parella, X. Fontrodona, J. Benet- Buchholz, M. Sola, L. Que Jr, E.V. Rybak-Akimova, M. Costas, Inorg. Chem. 46 (2007) 4997.
[41] (a) A. Panja, N.C. Jana, S. Adak, P. Brandão, L. Dlháň, J. Titiš, R. Boča, New J. Chem. 41 (2017) 3143;
(b) A. Panja, N.C. Jana, P. Brandão, Mol. Catal. 449 (2018) 49;
(c) A. Panja, N.C. Jana, P. Brandão, New J. Chem. 41 (2017) 9784.
[42] G.M. Sheldrick, SADABS, University of Go¨ttingen, Germany, 1996.
[43] G.M. Sheldrick, Acta Crystallogr., Sect. A Found Crystallogr. 64 (2008) 112.
[44] N.C. Jana, K. Pramanik, A. Bauzá, P. Brandão, M. Patra, A. Frontera, A. Panja, Polyhedron 124 (2017) 262.
[45] D. Bandyopadhyay, M. Layek, M. Fleck, R. Saha, C. Rizzoli, Inorg. Chim. Acta. 461 (2017) 174.
[46] S. Banerjee, R. Patra, P. Ghorai, P. Brandão, S.G. Chowdhury, P. Karmakar, A. Saha, New J. Chem. 42 (20) (2018) 16571.
[47] W. Cao, Y. Liu, T. Zhang, J. Jia, Polyhedron. 147 (2018) 62.
[48] A.T. Fiedler, A.A. Fischer, J. Biol. Inorg. Chem. 22 (2–3) (2017) 407.
[49] F.N. Karabulut, H.L. Feltham, S. Brooker, Dalton Trans. 47 (2018) 11749.
[50] A. Panja, Dalton Trans. 43 (2014) 7760.
[51] A. Panja, P. Guionneau, Dalton Trans. 42 (14) (2013) 5068.
[52] P. Chakraborty, S. Mohanta, Inorg. Chim. Acta. 435 (2015) 38.
[53] M.A. Goher, A.A. Youssef, F.A. Mautner, Polyhedron 25 (7) (2006) 1531.
[54] K. Ghosh, K. Harms, A. Bauzá, A. Frontera, S. Chattopadhyay, Dalton Trans. 47 (2) (2018) 331.
[55] L. Mandal, S. Mohanta, Dalton Trans. 43 (2014) 15737.
[56] H. Mori, N. Sakurai, S. Tanaka, H. Moriyama, T. Mori, H. Kobayashi, A. Kobayashi, Chem. Mater. 12 (2000) 2984.
[57] S. Sen, P. Talukder, S.K. Dey, S. Mitra, G. Rosair, D.L. Hughes, G.P.A. Yap, G. Pilet, V. Gramlich, T. Matsushita, Dalton Trans. (2006) 1758.
[58] A. Ray, G.M. Rosair, R. Kadam, S. Mitra, Polyhedron 28 (2009) 796.
[59] (a) N. Sarkar, K. Harms, A. Bauzá, A. Frontera, S. Chattopadhyay, ChemistrySelect. 2 (2017) 2975;
(b) K. Ghosh, K. Harms, S. Chattopadhyay, Polyhedron 112 (2016) 6.